ACS OMEGA

http://pubs.acs.org/journal/acsodf

Article

Impact of Thiol−Disulfide Balance on the Binding of Covid-19 Spike Protein with Angiotensin-Converting Enzyme 2 Receptor

Sanchita Hati and Sudeep Bhattacharyya*

Cite This: *ACS Omega* 2020, 5, 16292−16298

Read Online

ACCESS | Metrics & More | Article Recommendations

ABSTRACT: The novel coronavirus, severe acute respiratory syndrome coronavirus 2 (SARS-CoV-2), has led to an ongoing pandemic of coronavirus disease (COVID-19), which started in 2019. This is a member of Coronaviridae family in the genus *Betacoronavirus*, which also includes SARS-CoV and Middle East respiratory syndrome coronavirus (MERS-CoV). The angiotensin-converting enzyme 2 (ACE2) is the functional receptor for SARS-CoV and SARS-CoV-2 to enter the host cells. In particular, the interaction of viral spike proteins with ACE2 is a critical step in the viral replication cycle. The receptor-binding domain of the viral spike proteins and ACE2 have several cysteine residues. In this study, the role of thiol−disulfide balance on the interactions between SARS-CoV/CoV-2 spike proteins and ACE2 was investigated using molecular dynamics simulations. The study revealed that the binding affinity was significantly impaired when all of the disulfide bonds of both ACE2 and SARS-CoV/CoV-2 spike proteins were reduced to thiol groups. The impact on the binding affinity was less severe when the disulfide bridges of only one of the binding partners were reduced to thiols. This computational finding possibly provides a molecular basis for the differential COVID-19 cellular recognition due to the oxidative stress.

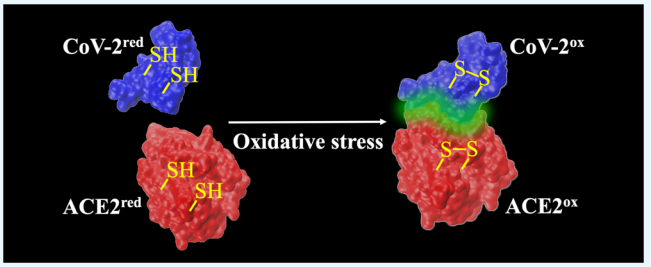

1. INTRODUCTION

The novel coronavirus known as severe acute respiratory syndrome coronavirus 2 (SARS-CoV-2) or simply COVID-19 is the seventh member of the coronavirus family.[1] The other two viruses in this family that infect humans are severe acute respiratory syndrome coronavirus (SARS-CoV) and Middle East respiratory syndrome coronavirus (MERS-CoV). These are positive-sense, single-strand enveloped RNA viruses. The coronavirus particles contain four main structural proteins: the spike, membrane, envelope, and nucleocapsid.[1,2] The spike protein protrudes from the envelope of the virion and consists of two subunits: a receptor-binding domain (RBD) that interacts with the receptor proteins of host cells and a second subunit that facilitates fusion of the viral membrane into the host cell membrane. Recent studies showed that the RBD of spike proteins of SARS-CoV and SARS-CoV-2 interact with angiotensin-converting enzyme 2 (ACE2). ACE2 belongs to the membrane-bound carboxydipeptidase family. It is attached to the outer surfaces of cells and is widely distributed in the human body. In particular, higher expression of ACE2 is observed in organs such as small intestine, colon, kidney, and heart, while ACE2 expression is comparatively lower in the liver and lungs.[3,4]

The role of oxidative stress on the binding of viral proteins on the host cell surface receptors is a relatively underexplored area of biomedical research.[5−10] Previous studies have indicated that the entry of viral glycoprotein is impacted by thiol−disulfide balance on the cell surface.[5,7−9,11,12] Any perturbations in the thiol−disulfide equilibrium are also found to deter the entry of viruses into their target cells.[5] The first step of the viral entry involves binding of the viral envelop protein onto a cellular receptor. This is followed by endocytosis, after which conformational changes of the viral protein help the induction of the viral protein into the endosomal membrane, finally releasing the viral content into the cell. These conformational changes are mediated by pH changes as well as the conversion of disulfide into the thiol group of the viral spike protein.[7] Several cell surface oxidoreductases[9] regulate the thiol−disulfide exchange, responsible for conformational changes of viral proteins needed for virus entry into host cells.

In the backdrop of a significant mortality rate for SARS-CoV-2 (hereinafter referred to as CoV-2) infection, it is important to know if the thiol−disulfide balance plays any role in the binding of the spike glycoprotein onto the host cell receptor protein ACE2. A recent study with the spike

Received: May 7, 2020
Accepted: June 5, 2020
Published: June 23, 2020

https://dx.doi.org/10.1021/acsomega.0c02125
ACS Omega 2020, 5, 16292−16298

```
CoV-2   RVQPTESIVRFPNITNLCPFGEVFNATRFASVYAWNRKRISNCVADYSVLYNSASFSTFK      60
CoV     ------------------PFGEVFNATKFPSVYAWERKKISNCVADYSVLYNSTFFSTFK      42
                          *********:* *****:**:**************: *****

CoV-2   CYGVSPTKLNDLCFTNVYADSFVIRGDEVRQIAPGQTGKIADYNYKLPDDFTGCVIAWNS      120
CoV     CYGVSATKLNDLCFSNVYADSFVVKGDDVRQIAPGQTGVIADYNYKLPDDFMGCVLAWNT      102
        ***** ********:********::**:********** ************ ***:***:

CoV-2   NNLDSKVGGNYNYLYRLFRKSNLKPFERDISTEIYQAGSTPCNGVEGFNCYFPLQSYGFQ      180
CoV     RNIDATSTGNYNYKYRYLRHGKLRPFERDISNVPFSPDGKPCTP-PALNCYWPLNDYGFY      161
        .*:*:.  ***** ** :*:.:*:*******.  :. ...**.   .:***:**:.***

CoV-2   PTNGVGYQPYRVVVLSFELLHAPATVCGPKKSTNLVKNKCVNFHHHHHH   229
CoV     TTTGIGYQPYRVVVLSFE------------------------------   179
         *.*:**************
```

Figure 1. Sequence alignment (generated by Clustal Omega[35]) between the receptor-binding domain of SARS-CoV and SARS-CoV-2 proteins. "*" represents the identical residues, ":" and "." represent strongly and weakly similar residues, respectively, and gap represents dissimilar residues. The cysteine residues are highlighted in yellow.

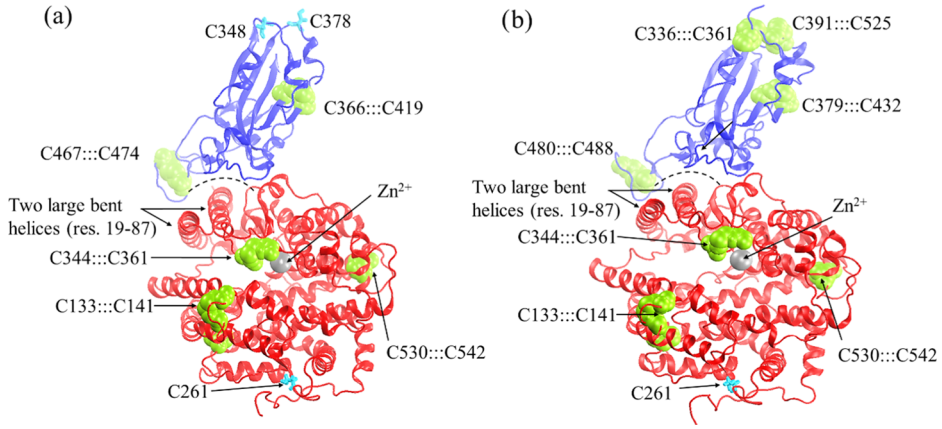

Figure 2. Structures of protein complexes: (a) SARS-CoV···ACE2 and (b) SARS-CoV-2···ACE2. All of the disulfide bridges between cysteine residues are shown in green van der Waals (vdW) spheres and thiol groups in cyan licorice.

glycoprotein of SARS-CoV (hereinafter referred to as CoV) has exhibited a complete redox insensitivity;[7] despite the reduction of all disulfide bridges of CoV to thiols, its binding to ACE2 remained unchanged.[7] However, this study did not probe the redox sensitivity of the ACE2 receptor. Thus, in the present study, we computationally investigated the redox state of both partners (ACE2 and CoV/CoV-2) on their binding affinities. The structure of CoV[13] and CoV-2[14,15] complexed with ACE2 are known, and the noncovalent interactions at the protein−protein interface[16] have been reported recently. Using these reported structures, molecular dynamics simulations and electrostatic field calculations were performed to explore the impact of thiol−disulfide balance on CoV/CoV-2 and ACE2 binding affinities. The structural and dynamical changes due to the alteration in the redox states of cysteines in the interacting proteins were analyzed, and their effects on binding free energies were studied.

2. RESULTS AND DISCUSSION

The molecular basis of the binding of spike proteins to ACE2 is known from X-ray crystallographic (SARS-CoV)[13] and cryo-electron microscopic (SARS-CoV-2)[16] studies. The sequence alignment of CoV and CoV-2 spike proteins showed a high sequence identity (>75%), indicating that their binding to ACE2 receptors will be similar (Figure 1). In both bound structures, the RBD of CoV and CoV-2 is found to be complexed with ACE2 (Figure 2). Both ACE2 and CoV-2 possess four disulfide bridges, whereas the CoV subunit has only two disulfide linkages (Table 1 and Figure 2a,b). Two large helices of ACE2 form a curved surface (Figure 2, illustrated by the dashed curved line) that interacts with the concave region of CoV or CoV-2 subunit.

2.1. Structural Changes along the Trajectory. In all cases, the simulation started with an equilibrated structure that was obtained after minimizing the neutralized solvated protein complex built from the experimentally determined structures. The evolution of the protein structure along the molecular dynamics (MD) trajectory was monitored by calculating the root-mean-square deviation (RMSD) of each structure from the starting structure as a frame of reference following the standard procedure.[17] Briefly, during the MD simulation, the protein coordinates were recorded for every 10 ps interval and an RMSD of each frame was calculated from the average root-mean-square displacement of backbone C_α atoms with respect to the initial structure. Then, the RMSD values, averaged over conformations stored during 1 ns time, were plotted against the simulated time (Figure 3). Compared to the starting structure, only a moderate backbone fluctuation was noted in all protein complexes during 20 ns simulations, and the maximum of RMSD was in the range of 2.0−3.8 Å (Table 2). The evolution of dynamics was smooth, and its stability was demonstrated by the standard deviation of the computed

https://dx.doi.org/10.1021/acsomega.0c02125
ACS Omega 2020, 5, 16292−16298

Table 1. Sequences of the Receptor-Binding Domain of SARS-CoV and SARS-CoV-2 Proteins[a]

Protein systems	PDB Code	Sequence
CoV^{ox}	3D0G	P:324 PFGEVFNATKFPSVYAWERKKISNCVADYSVLYNSTFFSTFKCYGVSATKLNDLCFSNVYA CYS 366···CYS 419 DSFVVKGDDVRQIAPGQTGVIADYNYKLPDDFMGCVLAWNTRNIDATSTGNYNYKYRY LRHGKLRPFERDISNVPFSPDGKPCTPPALNCYWPLNDYGFYTTTGIGYQPYRVVVLSFE E:502 CYS 467···CYS 474
$CoV\text{-}2^{ox}$	6M0J	CYS 336···CYS 361 T: 333 RVQPTESIVRFPNITNLCPFGEVFNATRFASVYAWNRKRISNCVADYSVLYNSASFSTFKCYGVSPTKLNDLCFTNVY CYS 379···CYS 432 ADSFVIRGDEVRQIAPGQTGKIADYNYKLPDDFTGCVIAWNSNNLDSKVGGNYNYLYRLFRKSNLKPFERDISTEIY CYS 391···CYS 525 QAGSTPCNGVEGFNCYFPLQSYGFQPTNGVGYQPYRVVVLSFELLHAPATVCGPKKSTNLVKNKCVNFHHHHHH G: 526 CYS 480···CYS 488

[a]The cysteine residues are highlighted in yellow and disulfide bonds are shown using black solid lines. The start and end residues in the crystal structures are numbered and highlighted in red. The gray highlighted residues are missing in the crystal structure.

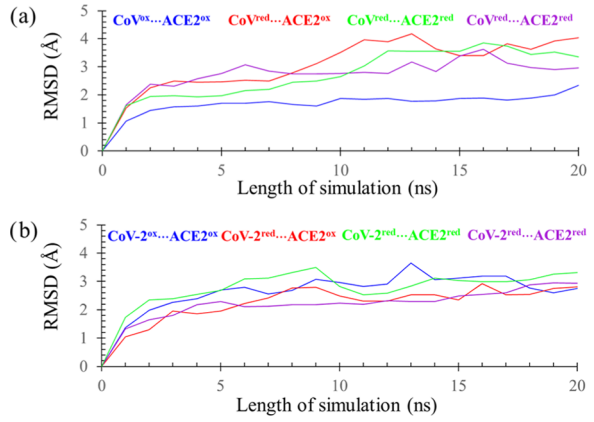

Figure 3. RMSDs, averaged over 1 ns MD simulation, of the protein complexes of ACE2 and SARS-CoV or SARS-CoV-2. Disulfide-containing proteins are referred to as oxidized with a shorthand notation of "ox", while thiol variants are denoted with "red" notation.

RMSDs, which was less than 0.3 Å. Taken together, the results of the simulations showed no unexpected structural deformation of the SARS-CoV/CoV-2···ACE2 complex in both, reduced (thiol groups) and oxidized (disulfide bonds) states (Table 2).

2.2. Thermal Fluctuations due to the Cleavage of Disulfide Bridges. The MD simulation results indicated that the flexibility of different structural elements of the interacting proteins altered upon the cleavage of disulfide bridges (oxidized state) producing sulfydryl (thiol) groups (reduced state). For each complex, the impact of the reduction of the disulfide bridges was probed by calculating residue-level root-mean-square fluctuations (RMSF) of C_α atoms with respect to the average structure from its MD simulation trajectory. Changes in the backbone flexibility due to complete reduction of all disulfides to thiols of both interacting proteins are shown in Figure 4a,b, where the backbone is color-coded to indicate the magnitude of thermal fluctuations. Larger and smaller backbone fluctuations are shown in red and blue, respectively, whereas the medium fluctuation regions are shown in green. The backbone fluctuation analysis demonstrated that the cleavage of disulfide bridges indeed affected the flexibility of the local regions as they became more dynamic (Figure 4b). A significant alteration in backbone flexibility was noticed at the interface of CoV and ACE2 subunits when both proteins are in the fully reduced states, i.e., all disulfides are changed to sulfydryl groups. As it is evident from Figure 4b, the helix (residues 52−64) of ACE2 became very mobile, due to the rupture of the nearby C344:::C361 disulfide. The second region belongs to the flexible loop consisting of residues 463−474 of the CoV subunit (residues 478−489 of the CoV-2 subunit), which interacts with the N-terminal segment of the ACE2. The cleavage of the disulfides C467:::C474 in CoV and C480:::C488 in CoV-2 resulted in higher thermal fluctuation.

2.3. Binding Study. The computed Gibbs binding free energy ($\Delta_{bind}G^\circ$) of protein complexes (Table 3) demonstrated that the binding of CoV or CoV-2 with ACE2 occurs because the attractive electrostatic interactions between the individual subunits prevail over the desolvation due to the complexation. The complex formation results in desolvation from proteins' surfaces at the protein−protein interface, thereby producing a positive $\Delta\Delta_{solv}G_{corr}$ for all protein systems (Table 3). For the formation of a stable protein−protein

https://dx.doi.org/10.1021/acsomega.0c02125
ACS Omega 2020, 5, 16292−16298

Table 2. Evolution of the Structure of the Protein Complexes for the Oxidized and Reduced Variants Observed during 20 ns Molecular Dynamics Simulations[a]

protein systems	number of disulfide moieties remaining	disulfide bridges present	RMSD (Å)	fluctuation (Å)
$CoV^{ox}\cdots ACE2^{ox}$	6	CoV: C366:::C419, C467:::C474, ACE2: C133:::C141, C344:::C361, C366:::C419, C530:::C542	2.0	0.2
$CoV^{red}\cdots ACE2^{ox}$	4	ACE2: C133:::C141, C344:::C361, C366:::C419, C530:::C542	3.8	0.3
$CoV^{ox}\cdots ACE2^{red}$	2	CoV: C366:::C419, C467:::C474	3.1	0.3
$CoV^{red}\cdots ACE2^{red}$	0	none	3.6	0.2
$CoV\text{-}2^{ox}\cdots ACE2^{ox}$	8	CoV-2: C336:::C361, C379:::C432, C391:::C525, C480:::C488, ACE2: C133:::C141, C344:::C361, C366:::C419, C530:::C542		
$CoV\text{-}2^{red}\cdots ACE2^{ox}$	4	ACE2: C133:::C141, C344:::C361, C366:::C419, C530:::C542	2.7	0.2
$CoV\text{-}2^{ox}\cdots ACE2^{red}$	4	CoV-2: C336:::C361, C379:::C432, C391:::C525, C480:::C488	2.8	0.2
$CoV\text{-}2^{red}\cdots ACE2^{red}$	0	none	3.1	0.2

[a]For each protein system, the "RMSD" column contains the average of the last 5 ns RMSD, and the "fluctuation" column represents the standard deviation computed based on the starting structure as a reference.

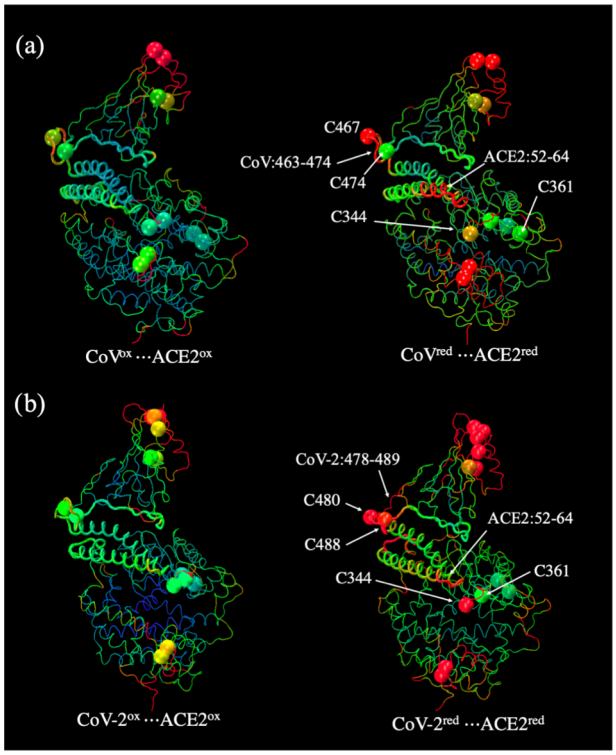

Figure 4. Change in residue-level RMSFs of C_α atoms in the oxidized and reduced protein complexes: (a) SARS-CoV···ACE2 and (b) SARS-CoV-2···ACE2. The cysteine residues, for each protein system (labeled in Figure 2), are highlighted as vdW spheres. The backbone as well as the cysteine residues are color-coded, large fluctuations are shown in red, and small fluctuations are in blue. The medium-scale fluctuations are shown in green.

complex, this energy has to be counterbalanced by the negative electrostatic interactions, $\Delta_{Coul}G$, between the interacting proteins.

When the disulfides of the RBD of CoV and CoV-2 were reduced to thiols, the impact of reduction on the binding of these two proteins with ACE2 was different. The computed $\Delta_{bind}G^\circ$ for $CoV^{ox}\cdots ACE2^{ox}$ and $CoV^{red}\cdots ACE2^{ox}$ are −7.3 and −11.2 kcal/mol, respectively (Table 3), indicating a slightly tighter binding of the reduced CoV RBD to ACE2. The experimentally known K_d value for the $CoV^{ox}\cdots ACE2^{ox}$ system is 325 nM,[14] which corresponds to a $\Delta_{bind}G^\circ$ value of −8.9 kcal/mol. Therefore, the computationally determined $\Delta_{bind}G^\circ$ for $CoV^{ox}\cdots ACE2^{ox}$ binding is comparable to the experimental value. Although there is no experimentally determined K_d available for the $CoV^{red}\cdots ACE2^{ox}$ system, the binding assay with CoV^{red} RBD was found to have no redox sensitivity for its binding to ACE2.[7] The small favorability of $CoV^{red}\cdots ACE2^{ox}$ binding, as observed from the computation, indicates that the reduction of CoV did not have much impact on its binding affinity for ACE2 and could explain the experimentally observed redox insensitivity.[7] In the case of CoV-2, its binding with ACE2 became less favorable when all of the disulfides of RBD were reduced to thiols. The computed Gibbs binding free energies were increased by ∼4.5 kcal/mol for the reduced CoV-2; $\Delta_{bind}G^\circ$ of $CoV\text{-}2^{ox}\cdots ACE2^{ox}$ and $CoV\text{-}2^{red}\cdots ACE2^{ox}$ are −10.4 and −6.0 kcal/mol, respectively.

Table 3. Various Components of the Gibbs Free Energy of Binding Calculated by Implicit Solvation and Adaptive-Basis Poisson−Boltzmann Solver (APBS)[a]

protein systems	Coulombic interaction free energy $\Delta_{Coul}G$	corrected solvation free energy difference $\Delta\Delta_{solv}G_{corr}$	Gibbs free energy of binding $\Delta_{bind}G^\circ$
$CoV^{ox}\cdots ACE2^{ox}$	−564.5	557.2	−7.3[b]
$CoV^{red}\cdots ACE2^{ox}$	−673.0	661.8	−11.2
$CoV^{ox}\cdots ACE2^{red}$	−696.6	693.1	−3.4
$CoV^{red}\cdots ACE2^{red}$	−528.4	580.4	52.0
$CoV\text{-}2^{ox}\cdots ACE2^{ox}$	−659.6	648.2	−10.4[c]
$CoV\text{-}2^{red}\cdots ACE2^{ox}$	−638.2	632.2	−6.0
$CoV\text{-}2^{ox}\cdots ACE2^{red}$	−531.9	528.1	−3.8
$CoV\text{-}2^{red}\cdots ACE2^{red}$	−655.3	712.6	57.3

[a]All energies are expressed in kcal/mol. An estimated uncertainty of 1−3 kcal/mol was determined for the computed Gibbs free energy. [b]An experimental value of −10.3 kcal/mol was obtained for SARS-CoV by Lan et al.[34] [c]An experimental K_d value of −10.4 kcal/mol for SARS-CoV-2···ACE2 complex, reported by Wang et al.,[15] was used as correction in eq 3.

In contrast, the reduction of disulfides of ACE2 impaired the binding significantly for both CoV and CoV-2 proteins. The Gibbs binding free energies of viral spike proteins CoV and CoV-2 with $ACE2^{red}$, namely, $CoV^{ox}\cdots ACE2^{red}$ and $CoV\text{-}2^{ox}\cdots ACE2^{red}$ are −3.4 and −3.8 kcal/mol, respectively. These $\Delta_{bind}G^\circ$ values are ∼4 to 6 kcal/mol more positive than what were observed for the oxidized forms of ACE2 (i.e., $CoV^{ox}\cdots ACE2^{ox}$ and $CoV\text{-}2^{ox}\cdots ACE2^{ox}$ in Table 3). However, when all disulfides in CoV/CoV-2 as well as ACE2 were reduced to thiols, the binding became thermodynamically unfavorable. In

https://dx.doi.org/10.1021/acsomega.0c02125
ACS Omega 2020, 5, 16292−16298

both cases, the binding free energies have positive values; $\Delta_{bind}G^{\circ}$ of CoV^{red}···ACE2^{red} and CoV-2^{red}···ACE2^{red} are 52.0 and 57.3 kcal/mol, respectively. These results indicate that the binding will be severely impacted, when the disulfides of both interacting proteins are converted to thiols. This finding is potentially significant as it indicates that the cleavage of disulfide bridges in ACE2 has a significant destabilizing effect on the spike protein binding.

2.4. Molecular Basis of the Impaired Binding. The conjoined two helices of ACE2 (residues 19−53 and residues 56−94) form a complementary shape (Figure 5) that fits into

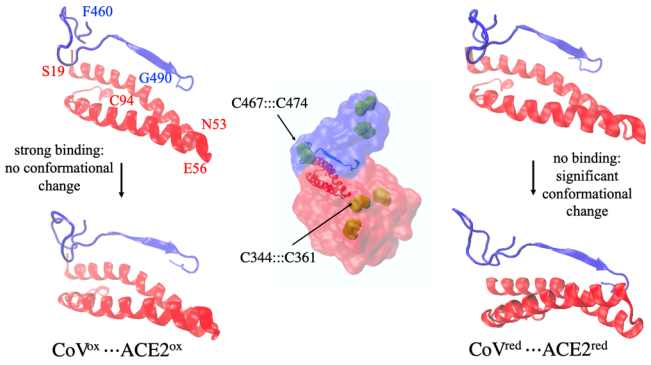

Figure 5. Comparison of the conformational change at the protein−protein interface in CoV^{ox}···ACE2^{ox} (left) and CoV^{red}···ACE2^{red} (right). CoV and ACE2 subunits in the complex are shown in blue and red colors, respectively, at the center. The structural motif containing the two helices of ACE2 and a β sheet of the CoV (or CoV-2) was monitored before (top) and after (bottom) 20 ns MD simulation. The left and right panels show the difference in conformational changes in the oxidized form (CoV^{ox}···ACE2^{ox}) and reduced form (CoV^{red}···ACE2^{red}), respectively.

the concave-shaped loop-β-sheet-loop motif (residues 460−490 of CoV and residues 475−505 of CoV-2) of RBD of viral spike proteins. The loss of disulfide bridges in ACE2 had a strong impact on the junction of the two conjoined helices (Figure 5, CoV^{red}···ACE2^{red}). This region is close to the disulfide bridge C344:::C361, and its cleavage has a significant impact on the shape complementarity at the protein−protein interface. Similarly, the loss of C467:::C474 disulfide in CoV (C480:::C488 in CoV-2) resulted in a significant conformational change in the loop region, which was displaced away from the protein−protein interface by ∼6 Å, indicating a reduced binding interaction as confirmed by the binding free energy calculations. This conformational change as well as the alteration in the backbone flexibility (Figure 4) must have resulted in impaired binding of CoV/CoV-2 with ACE2.

3. CONCLUSIONS

The study found that the reduction of all disulfides into sulfydryl groups completely impairs the binding of SARS-CoV/CoV-2 spike protein to ACE2. This is evident from the positive Gibbs energy of binding ($\Delta_{bind}G^{\circ}$) obtained for both CoV^{red}···ACE2^{red} and CoV-2^{red}···ACE2^{red} complexes. When the disulfides of only ACE2 were reduced to sulfydryl groups, the binding becomes weaker, as $\Delta_{bind}G^{\circ}$ becomes less negative by 4−6 kcal/mol with respect to the fully oxidized systems. On the other hand, the reduction of disulfides of the RBD of CoV-2 has comparatively less effect on $\Delta_{bind}G^{\circ}$, while the reduction of disulfides in CoV RBD does not impact the binding with ACE2. This finding is consistent with the observed redox insensitivity of the binding between CoV and ACE2.[7]

The redox environment of cell surface receptors is regulated by the thiol−disulfide equilibrium in the extracellular region.[12,18] This is maintained by glutathione transporters,[19] a number of oxidoreductases[12] including protein disulfide isomerase,[8] and several redox switches.[12] Under oxidative stress, the extracellular environment becomes oxidation-prone resulting in more disulfide formation on protein surfaces.[12] Therefore, under severe oxidative stress, the cell surface receptor ACE2 and RBD of the intruding viral spike protein are likely to be present in its oxidized form having predominantly disulfide linkages. This computational study shows that under oxidative stress, the lack of a reducing environment would result in significantly favorable binding of the viral protein on the cell surface ACE2. In terms of energetics, this computational study demonstrates that the oxidized form of proteins with disulfide bridges would cause more than 50 kcal/mol of decrease in Gibbs binding free energy. Furthermore, ACE2, which the viral spike proteins latch on to, is known to be a key player in the remedial of oxidative stress.[20] Binding of the viral protein will prevent the key catalytic function of ACE2 of converting angiotensin 2 (a strong activator of oxidative stress) to angiotensin 1−7 thereby creating a vicious circle of enhanced viral attack. In summary, the present study demonstrates that the absence of or reduced oxidative stress would have a significant beneficial effect during the early stage of viral infection by preventing viral protein binding on the host cells.

4. METHODOLOGY

4.1. Computational Setup. Setting up of protein systems and all structural manipulations were carried out using visual molecular dynamics (VMD).[21] Disulfide groups were modified to thiols during the setting up of structures using standard VMD scripts. Molecular optimization and dynamics (MD) simulations were carried out using nanoscale molecular dynamics (NAMD) package using CHARMM36 force field.[22−26] During MD simulations, electrostatic energy calculations were carried out using the particle mesh Ewald method.[27] Backbone root-mean-square-deviation (RMSD) calculations were performed using VMD. Protein−protein interactions were studied using adaptive-basis Poisson−Boltzmann solver (APBS).[28] Electrostatic field calculations were performed using PDB 2PQR program suit.[29]

4.2. Molecular Dynamics Simulations. All simulations were performed using the structure of ACE2 bound SARS-CoV (PDB entry: 3D0G)[13] and SARS-CoV-2 (PDB entry: 6M0J).[15] In all simulations, set up of protein complex systems was carried out following protocols used in the previous studies from this lab.[17,30] Briefly, hydrogens were added using the HBUILD module of CHARMM. Ionic amino acid residues were maintained in a protonation state corresponding to pH 7. The protonation state of histidine residues was determined by computing the pK_a using the Propka option of PDB 2PQR. The protein structures were explicitly solvated with water of the TIP3P model and neutralized by adding with 24 sodium atoms. The prepared solvated protein complexes were of dimensions 92 Å × 132 Å × 104 Å for SARS-CoV and 94 Å × 144 Å × 100 Å for SARS-CoV-2 systems.[21]

All systems were subjected to equilibration for 50 ps. Following equilibration, 20 ns MD simulations were performed for each system. The velocities and positions of atoms during

https://dx.doi.org/10.1021/acsomega.0c02125
ACS Omega 2020, 5, 16292−16298

Scheme 1

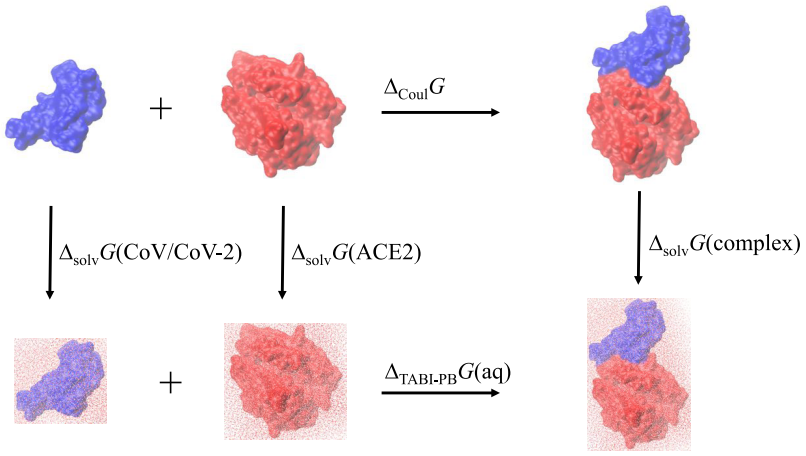

dynamics were calculated using the velocity Verlet integration algorithm[31] using a time step of 2.0 fs. All simulations were run with NAMD implementation of Langevin dynamics[32] at a constant temperature of 298 K using periodic boundary conditions. To model, nonbonding interactions, a switching function was turned on with a "switchdist" of 10 Å, a cutoff of 14 Å, and a "pairlistdist" of 16 Å.

4.3. Binding Free Energy Calculations. Gibbs free energies of binding between the ACE2 and SARS-CoV or CoV-2 proteins were calculated using APBS, a standardized method of a treecode-accelerated boundary integral Poisson–Boltzmann (TABI-PB) equation solver.[33] In this method, the protein surface is triangulated and electrostatic surface potentials are computed. The discretization of surface potentials is utilized to compute the net energy due to solvation as well as electrostatic interactions between the two protein subunits, as outlined in the thermodynamic scheme (Scheme 1). Following Scheme 1, the free energy of binding of the two protein fragments in water can be expressed as a sum of two components (eq 1)

$$\Delta_{bind}G_{TABI-PB} = \Delta_{Coul}G + \Delta\Delta_{solv}G \quad (1)$$

where $\Delta_{Coul}G$ represents the Coulombic (electrostatic) interactions between the proteins occurring at the protein–protein interface (Scheme 1) and $\Delta\Delta_{solv}G$ is the difference of the solvation energies between the complex and the corresponding free proteins

$$\Delta\Delta_{solv}G = \Delta_{solv}G(\text{complex}) - \Delta_{solv}G(\text{CoV/CoV-2}) - \Delta_{solv}G(\text{ACE2}) \quad (2)$$

However, the solvation calculation used only part of the entire spike protein as well as the ACE2; therefore, $\Delta_{bind}G_{TABI\text{-}PB}$ was calibrated by correcting $\Delta\Delta_{solv}G$ using experimentally known binding free energy of ACE2···CoV-2

$$\Delta G_{corr} = RT \ln K_d - \Delta_{bind}G_{TABI-PB} \quad (3)$$

where K_d = 37 nM is the experimental dissociation constant.[16]

The corrected free energy of the solvation

$$\Delta\Delta_{solv}G_{corr} = \Delta\Delta_{solv}G + \Delta G_{corr} \quad (4)$$

Using ΔG_{corr} and eq 4, the corrected binding free energy, $\Delta_{bind}G^{\circ}$, of all protein complexes is expressed by

$$\Delta_{bind}G^{\circ} = \Delta_{bind}G_{TABI-PB} + \Delta G_{corr} = \Delta_{Coul}G + \Delta\Delta_{solv}G + \Delta G_{corr} \quad (5)$$

As shown in eq 4, the combination of the last two terms in eq 5 is equal to $\Delta\Delta_{solv}G_{corr.}$ Therefore, eq 5 can be simplified as

$$\Delta_{bind}G^{\circ} = \Delta_{Coul}G + \Delta\Delta_{solv}G_{corr} \quad (6)$$

AUTHOR INFORMATION

Corresponding Author

Sudeep Bhattacharyya − *Department of Chemistry, University of Wisconsin—Eau Claire, Eau Claire, Wisconsin 54701, United States;* orcid.org/0000-0002-3960-1239; Email: bhattas@uwec.edu

Author

Sanchita Hati − *Department of Chemistry, University of Wisconsin—Eau Claire, Eau Claire, Wisconsin 54701, United States*

Complete contact information is available at: https://pubs.acs.org/10.1021/acsomega.0c02125

Funding

This work was supported in part by the National Institute of Health (grant number 1R15GM117510-01 to S.H. and S.B.).

Notes

The authors declare no competing financial interest.

ACKNOWLEDGMENTS

We acknowledge computational support from the Blugold Super Computing Cluster (BGSC) of the University of Wisconsin—Eau Claire.

ABBREVIATIONS USED

ACE, angiotensin-converting enzyme; CoV, coronavirus; MD, molecular dynamics; RBD, receptor-binding domain; TABI-PB, treecode-accelerated boundary integral Poisson–Boltzmann

REFERENCES

(1) Schoeman, D.; Fielding, B. C. Coronavirus envelope protein: current knowledge. *Virol. J.* **2019**, *16*, No. 69.

(2) Fehr, A. R.; Perlman, S. Coronaviruses: an overview of their replication and pathogenesis. *Methods Mol. Biol.* **2015**, *1282*, 1–23.

(3) Chen, Y.; Guo, Y.; Pan, Y.; Zhao, Z. J. Structure analysis of the receptor binding of 2019-nCoV. *Biochem. Biophys. Res. Commun.* **2020**, *525*, 135−140.
(4) Xu, H.; Zhong, L.; Deng, J.; Peng, J.; Dan, H.; Zeng, X.; Li, T.; Chen, Q. High expression of ACE2 receptor of 2019-nCoV on the epithelial cells of oral mucosa. *Int. J. Oral Sci.* **2020**, *12*, No. 8.
(5) Ryser, H. J.; Levy, E. M.; Mandel, R.; DiSciullo, G. J. Inhibition of human immunodeficiency virus infection by agents that interfere with thiol-disulfide interchange upon virus-receptor interaction. *Proc. Natl. Acad. Sci. U.S.A.* **1994**, *91*, 4559−4563.
(6) Gallina, A.; Hanley, T. M.; Mandel, R.; Trahey, M.; Broder, C. C.; Viglianti, G. A.; Ryser, H. J. Inhibitors of protein-disulfide isomerase prevent cleavage of disulfide bonds in receptor-bound glycoprotein 120 and prevent HIV-1 entry. *J. Biol. Chem.* **2002**, *277*, 50579−50588.
(7) Lavillette, D.; Barbouche, R.; Yao, Y.; Boson, B.; Cosset, F. L.; Jones, I. M.; Fenouillet, E. Significant redox insensitivity of the functions of the SARS-CoV spike glycoprotein: comparison with HIV envelope. *J. Biol. Chem.* **2006**, *281*, 9200−9204.
(8) Pan, S.; Chen, H. H.; Correia, C.; Dai, H.; Witt, T. A.; Kleppe, L. S.; Burnett, J. C., Jr.; Simari, R. D. Cell surface protein disulfide isomerase regulates natriuretic peptide generation of cyclic guanosine monophosphate. *PLoS One* **2014**, *9*, No. e112986.
(9) Mathys, L.; Balzarini, J. The role of cellular oxidoreductases in viral entry and virus infection-associated oxidative stress: potential therapeutic applications. *Expert Opin. Ther. Targets* **2016**, *20*, 123−143.
(10) Camini, F. C.; da Silva Caetano, C. C.; Almeida, L. T.; de Brito Magalhães, C. L. Implications of oxidative stress on viral pathogenesis. *Arch. Virol.* **2017**, *162*, 907−917.
(11) Fenouillet, E.; Barbouche, R.; Jones, I. M. Cell entry by enveloped viruses: redox considerations for HIV and SARS-coronavirus. *Antioxid. Redox Signaling* **2007**, *9*, 1009−1034.
(12) Yi, M. C.; Khosla, C. Thiol-Disulfide Exchange Reactions in the Mammalian Extracellular Environment. *Annu. Rev. Chem. Biomol. Eng.* **2016**, *7*, 197−222.
(13) Li, F. Structural analysis of major species barriers between humans and palm civets for severe acute respiratory syndrome coronavirus infections. *J. Virol.* **2008**, *82*, 6984−6991.
(14) Wrapp, D.; Wang, N.; Corbett, K. S.; Goldsmith, J. A.; Hsieh, C. L.; Abiona, O.; Graham, B. S.; McLellan, J. S. Cryo-EM structure of the 2019-nCoV spike in the prefusion conformation. *Science* **2020**, *367*, 1260−1263.
(15) Wang, Q.; Zhang, Y.; Wu, L.; Niu, S.; Song, C.; Zhang, Z.; Lu, G.; Qiao, C.; Hu, Y.; Yuen, K. Y.; Wang, Q.; Zhou, H.; Yan, J.; Qi, J. Structural and Functional Basis of SARS-CoV-2 Entry by Using Human ACE2. *Cell* **2020**, *181*, 894−904.e9.
(16) Yan, R.; Zhang, Y.; Li, Y.; Xia, L.; Guo, Y.; Zhou, Q. Structural basis for the recognition of SARS-CoV-2 by full-length human ACE2. *Science* **2020**, *367*, 1444−1448.
(17) Adams, L. M.; Andrews, R. J.; Hu, Q. H.; Schmit, H. L.; Hati, S.; Bhattacharyya, S. Crowder-Induced Conformational Ensemble Shift in Escherichia coli Prolyl-tRNA Synthetase. *Biophys. J.* **2019**, *117*, 1269−1284.
(18) Bechtel, T. J.; Weerapana, E. From structure to redox: The diverse functional roles of disulfides and implications in disease. *Proteomics* **2017**, *17*, No. 1600391.
(19) Ballatori, N.; Krance, S. M.; Marchan, R.; Hammond, C. L. Plasma membrane glutathione transporters and their roles in cell physiology and pathophysiology. *Mol. Aspects Med.* **2009**, *30*, 13−28.
(20) Xia, H.; Suda, S.; Bindom, S.; Feng, Y.; Gurley, S. B.; Seth, D.; Navar, L. G.; Lazartigues, E. ACE2-mediated reduction of oxidative stress in the central nervous system is associated with improvement of autonomic function. *PLoS One* **2011**, *6*, No. e22682.
(21) Humphrey, W.; Dalke, A.; Schulten, K. VMD: visual molecular dynamics. *J. Mol. Graphics* **1996**, *14*, 33−38.
(22) Guvench, O.; Hatcher, E.; Venable, R. M.; Pastor, R. W.; MacKerell, A. D. CHARMM Additive All-Atom Force Field for Glycosidic Linkages between Hexopyranoses. *J. Chem. Theory Comput.* **2009**, *5*, 2353−2370.
(23) Raman, E. P.; Guvench, O.; MacKerell, A. D., Jr. CHARMM additive all-atom force field for glycosidic linkages in carbohydrates involving furanoses. *J. Phys. Chem. B* **2010**, *114*, 12981−12994.
(24) Guvench, O.; Mallajosyula, S. S.; Raman, E. P.; Hatcher, E.; Vanommeslaeghe, K.; Foster, T. J.; Jamison, F. W., II; Mackerell, A. D., Jr. CHARMM additive all-atom force field for carbohydrate derivatives and its utility in polysaccharide and carbohydrate-protein modeling. *J. Chem. Theory Comput.* **2011**, *7*, 3162−3180.
(25) Best, R. B.; Zhu, X.; Shim, J.; Lopes, P. E. M.; Mittal, J.; Feig, M.; MacKerell, A. D. Optimization of the additive CHARMM all-atom protein force field targeting improved sampling of the backbone φ, ψ and side-chain $\chi(1)$ and $\chi(2)$ dihedral angles. *J. Chem. Theory Comput.* **2012**, *8*, 3257−3273.
(26) Mallajosyula, S. S.; Guvench, O.; Hatcher, E.; Mackerell, A. D., Jr. CHARMM Additive All-Atom Force Field for Phosphate and Sulfate Linked to Carbohydrates. *J. Chem. Theory Comput.* **2012**, *8*, 759−776.
(27) Essmann, U.; Perera, L.; Berkowitz, M. L.; et al. A smooth particle mesh Ewald method. *J. Chem. Phys.* **1995**, *103*, 8577.
(28) Jurrus, E.; Engel, D.; Star, K.; Monson, K.; Brandi, J.; Felberg, L. E.; Brookes, D. H.; Wilson, L.; Chen, J.; Liles, K.; Chun, M.; Li, P.; Gohara, D. W.; Dolinsky, T.; Konecny, R.; Koes, D. R.; Nielsen, J. E.; Head-Gordon, T.; Geng, W.; Krasny, R.; Wei, G. W.; Holst, M. J.; McCammon, J. A.; Baker, N. A. Improvements to the APBS biomolecular solvation software suite. *Protein Sci.* **2018**, *27*, 112−128.
(29) Dolinsky, T. J.; Czodrowski, P.; Li, H.; Nielsen, J. E.; Jensen, J. H.; Klebe, G.; Baker, N. A. PDB2PQR: expanding and upgrading automated preparation of biomolecular structures for molecular simulations. *Nucleic Acids Res.* **2007**, *35*, W522−W525.
(30) Johnson, J. M.; Sanford, B. L.; Strom, A. M.; Tadayon, S. N.; Lehman, B. P.; Zirbes, A. M.; Bhattacharyya, S.; Musier-Forsyth, K.; Hati, S. Multiple pathways promote dynamical coupling between catalytic domains in Escherichia coli prolyl-tRNA synthetase. *Biochemistry* **2013**, *52*, 4399−4412.
(31) Verlet, L. Computer "experiments" on classic fluids. I. Thermodynamical properties of Lennard-Jones molecules. *Phys. Rev.* **1967**, *159*, 98−103.
(32) Phillips, J. C.; Braun, R.; Wang, W.; Gumbart, J.; Tajkhorshid, E.; Villa, E.; Chipot, C.; Skeel, R. D.; Kalé, L.; Schulten, K. Scalable molecular dynamics with NAMD. *J. Comput. Chem.* **2005**, *26*, 1781−1802.
(33) Geng, W.; Krasny, R. A treecode-accelerated boundary integral Poisson−Boltzmann solver for electrostatics of solvated biomolecules. *J. Comput. Phys.* **2013**, *247*, 62−78.
(34) Lan, J.; Ge, J.; Yu, J.; Shan, S.; Zhou, H.; Fan, S.; Zhang, Q.; Shi, X.; Wang, Q.; Zhang, L.; Wang, X. Structure of the SARS-CoV-2 spike receptor-binding domain bound to the ACE2 receptor. *Nature* **2020**, *581*, 215−220.
(35) Madeira, F.; Park, Y. M.; Lee, J.; Buso, N.; Gur, T.; Madhusoodanan, N.; Basutkar, P.; Tivey, A. R. N.; Potter, S. C.; Finn, R. D.; Lopez, R. The EMBL-EBI search and sequence analysis tools APIs in 2019. *Nucleic Acids Res.* **2019**, *47*, W636−W641.

https://dx.doi.org/10.1021/acsomega.0c02125
ACS Omega 2020, 5, 16292−16298